J. Magn. Soc. Jpn., **40**, 13-17 (2016) <Paper>

Structure and Magnetic Properties of (001) Oriented CoPt-Ag and CoPd-Ag Alloy Films

T. Nagata, Y. Tokuoka, T. Kato, D. Oshima*, and S. Iwata*
Graduate School of Engineering, Nagoya University, *Furo-cho, Chikusa-ku, Nagoya 464–8603, Japan*
*EcoTopia Science Institute, Nagoya University, *Furo-cho, Chikusa-ku, Nagoya 464–8603, Japan*

20-nm-thick $(CoPt)_{100-x}Ag_x$ and $(CoPd)_{100-x}Ag_x$ (001) films (x = 0–20) were grown on MgO(001) substrate at a temperature of 300°C by molecular beam epitaxy, and their crystal structure and magnetic properties were compared with those of FePt-Ag and FePd-Ag films [Y. Tokuoka *et al.*: *J. Appl. Phys.*, **115**, 17B716 (2014)] for the systematic study of the effect of Ag addition into transition metal – noble metal alloy films. For the CoPt-Ag, the addition of 5% Ag increased perpendicular magnetic anisotropy (PMA) and coercivity. However, for the CoPd-Ag, Ag addition enhanced neither the PMA nor the coercivity. Structural analysis of the CoPt-Ag and CoPd-Ag films revealed that Ag addition promoted $L1_0$ phase ordering for CoPt-Ag, while $L1_0$ ordering was not found in CoPd-Ag. Although there were some similarities in the effect of Ag addition between CoPt-Ag and FePt-Ag, such as increased PMA, coercivity, and $L1_0$ ordering, there were different trends in PMA and $L1_0$ ordering between CoPd-Ag and FePd-Ag, except that both films showed reduced coercivity with Ag addition. Ag segregation and $L1_0$ ordering are considered important factors to explain the variations of structure and magnetic properties with Ag addition.

Key words: perpendicular magnetic anisotropy, Ag segregation, CoPt, CoPd

1. Introduction

Tetoragonal $L1_0$ phase magnetic materials, e.g., FePt and CoPt, have been extensively studied as potential candidates for future high-density perpendicular recording media because of their extremely large perpendicular magnetic anisotropies (PMA). However, for the practical application of these materials, there still remain challenges such as fabrication of nano-sized grains, control of (001) orientation, and lowering the ordering temperature of $L1_0$ phase[1), 2)]. One of the effective ways to realize these requirements is the addition of the third element. Ag or Cu addition into FePt is known to be effective to reduce its $L1_0$ ordering temperature[3)–6)]. The addition of Ag into CoPt is also known to promote $L1_0$ ordering and (001) orientation, which is crucial to obtain the large PMA[7), 8)]. Moreover, it is reported that the ordering temperature of FePd is reduced by insertion of the Ag underlayer[9)].

We have also studied FePt-Ag and FePd-Ag films to investigate the effect of Ag addition into $L1_0$ phase magnetic materials[10)–12)], and reported Ag addition to FePt with the amount of around 10 at. % is effective to promote $L1_0$ ordering and granular growth of FePt, resulting in the increase of the PMA and coercivity of the film normal direction. From the structural analysis and magnetic properties measurements, it was concluded that the Ag is segregated from FePt, and this phase separation promotes $L1_0$ ordering and granular growth of FePt[12)]. Unlike the case of FePt-Ag, Ag addition into FePd does not contribute to the corecivity increase and granular growth, and the formation of FePd-Ag alloy was observed[12)]. This suggests that the phase separation is a key factor to control the microstructure of $L1_0$ phase magnetic materials and to obtain suitable magnetic properties for the perpendicular recording media.

Recently, L. Zhang *et al.* reported that FePt-Ag:C films have large PMA and small grain size of around 6 nm[13)]. They reported a substantial increase of the PMA of FePt by the Ag addition, and the increase of the PMA is considered to be due to the phase separation of Ag and FePt by the heat treatment, in which the $L1_0$ ordering of FePt is promoted through the atom replacement by the Ag diffusion[14)].

In this paper, CoPt-Ag and CoPd-Ag films have been studied in detail for the systematic understanding of the effect of Ag addition in 3*d* transition metal and noble metal alloy films. Although no ordered phase is reported in bulk CoPd[15)], metastable $L1_0$ phase CoPd was reported in evaporated CoPd alloy films[16)]. The phase separation of Ag and CoPt or CoPd as well as the enhancement of $L1_0$ ordering by Ag addition are discussed. In addition to the structural analysis, the relationship between the structure and magnetic properties is studied in detail. Furthermore, the effect of Ag addition into CoPt and CoPd is compared with the results of previously reported FePt-Ag and FePd-Ag.

2. Experiment

In our previous study, 5 nm-thick $(FePt)_{100-x}Ag_x$ and $(FePd)_{100-x}Ag_x$ were grown directly on MgO(001) substrates[12)]. However, *c*–axis orientation of 5 nm-thick CoPt on MgO(001) was poor compared to the FePt-Ag, due to the lattice mismatch between CoPt and MgO. Thus in this study, 20 nm-thick $(CoPt)_{100-x}Ag_x$ and $(CoPd)_{100-x}Ag_x$ films (x = 0–20) were grown by molecular beam epitaxy (MBE) method. The CoPt-Ag was grown directly on MgO(001) substrates while CoPd-Ag was

grown on 10 nm thick Pd (001) buffer layer to reduce the lattice mismatching between CoPd and MgO(001) substrate. The Pd buffer layer was grown at room temperature, and CoPt and CoPd layers were grown at 300°C. Co, Pt (Pd), and Ag were co-evaporated from independently controlled e-beam sources, for which the deposition rate of each element was monitored by quartz thickness monitors. During the deposition, the MBE chamber was kept at a pressure of less than 3×10^{-7} Pa. Before the deposition, the MgO substrate was cleaned by 1 keV Ar^+ ion bombardment followed by the heat treatment at 1000°C in the MBE chamber.

The film structure was characterized by *in-situ* reflection high energy electron diffraction (RHEED) and *ex-situ* X-ray diffraction (XRD) using Cu $K\alpha$ radiation source (λ = 0.15418 nm). Hysteresis loops and magnetic anisotropies were measured by an alternating gradient field magnetometer and a torque magnetometer, respectively. The surface topography was checked by the atomic force microscopy (AFM).

3. Results and Discussions

3.1 Crystal structure and surface morphology

Figure 1 shows ω–2θ XRD profiles of $(CoPt)_{100-x}Ag_x$ and $(CoPd)_{100-x}Ag_x$ grown at 300°C. In the profiles of CoPt-Ag, 001 superlattice and 002 fundamental diffractions were clearly seen, which indicates the existence of (001) oriented $L1_0$ phase. Moreover, CoPt 001 peak intensity increased by adding Ag and no significant changes in the peak positions of CoPt 001 and 002 with the Ag addition were found. In the profiles of CoPd-Ag, Pd 002 and CoPd 002 peaks indicate the (001) oriented growth of Pd buffer and CoPd layers on the MgO(001) substrate. At x = 0, there exist reflections indicated as "*" in the figure around 2θ = 16 deg and 32 deg. The lattice spacings estimated from these peaks are 0.55 nm and 0.28 nm, respectively, which coincide with 3- and 1.5-times of CoPd 002 spacing of 0.184 nm. This suggests the existence of the long range order structure along the CoPd [001] direction. With the increase of Ag content, this long range order structure of CoPd disappeared. The lattice constant estimated from the CoPd 002 was 0.366 nm, and the peak position of CoPd 002 did not change significantly with increasing Ag content.

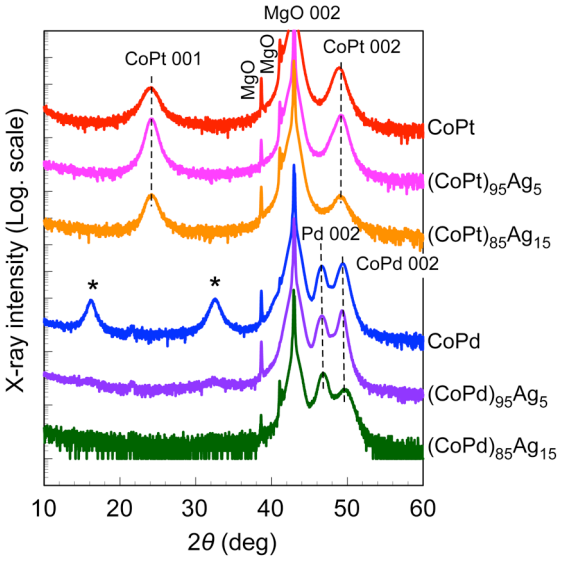

Fig. 1 ω–2θ XRD profiles of $(CoPt)_{100-x}Ag_x$ and $(CoPd)_{100-x}Ag_x$ alloy films (x = 0, 5, and 15) grown at 300°C. X-ray scattering vector is normal to the film surface. For the profile of CoPd, there exist reflections indicated as "*" around 2θ = 16 deg and 32 deg. The lattice spacings estimated from these peaks are 0.55 nm and 0.28 nm, respectively, which coincide with 3- and 1.5-times of CoPd 002 spacing of 0.184 nm.

The reciprocal space mapping of CoPd also showed the existence of the long range order structure along [001] direction. Figure 2 shows the reciprocal space mapping for a slice of (110) plane of CoPd grown on MgO (001) at 300°C. The Q_x and Q_z are along MgO[110] and [001] directions, respectively, and the radial component of the scattering vector was calculated as:

$$\sqrt{Q_x^2 + Q_z^2} = \frac{2\sin\theta}{\lambda}, \qquad (1)$$

where λ = 1.5418 Å and θ is Bragg angle.

The diffraction spots at Q_z = 0.18 $Å^{-1}$ and 0.36 $Å^{-1}$ correspond to the peaks indicated as "*" in Fig. 1. Besides these spots, several diffraction spots, such as (Q_x, Q_z) = (–0.37 $Å^{-1}$, 0.63 $Å^{-1}$) and (0.37 $Å^{-1}$, 0.63 $Å^{-1}$) are seen, suggesting the existence of the long range order structure along CoPd [001] direction. More detail structural analysis is necessary to elucidate the

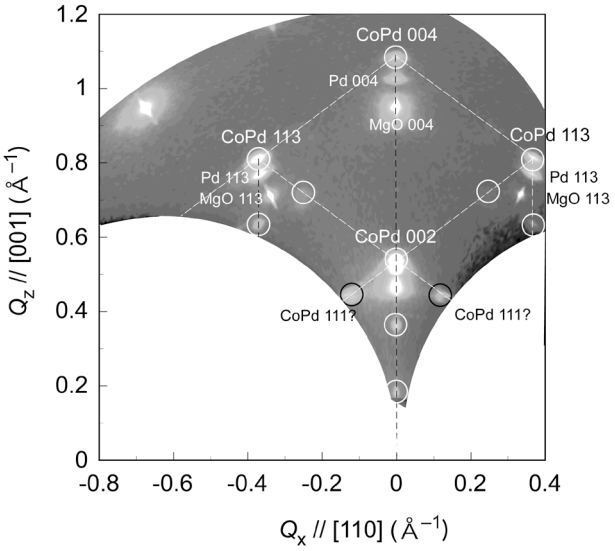

Fig. 2 Reciprocal space mapping of (110) plane of CoPd film grown on MgO (001) at 300°C.

structure of CoPd alloy films, but at present we consider two possibilities: atomic layered structure along [001] direction with a period of 3 times of 002 spacing (0.184 nm) or periodic anti-phase domain boundary similar to that observed in CuAu[17], Cu_3Pd[18], etc.

Figure 3 shows in-plane ϕ–$2\theta\chi$ XRD profiles of $(CoPt)_{100-x}Ag_x$ and $(CoPd)_{100-x}Ag_x$ with x = 0 and 15. The profiles were taken under the condition that the X-ray scattering vector is along MgO [100] direction. Besides the reflection of MgO 200, intense peak from CoPt 200 or CoPd 200 is seen in the profile at x = 0. No superlattice reflections of CoPt and CoPd were seen in the profiles. The addition of Ag did not significantly change the peak position of CoPt 200 and CoPd 200, and Ag 200 peak was seen in the profiles at x = 15. The lattice constants a estimated from the CoPt 200 and CoPd 200 peaks were 0.380 nm and 0.379 nm, respectively. From these structural analyses, we concluded that the Ag is segregated from CoPt or CoPd, and promotes $L1_0$ ordering of CoPt. $L1_0$-CoPt is well known as a stable phase near equiatomic composition of Co and Pt, while $L1_0$-CoPd is reported to be metastable[16]. Although, the addition of the third element, e.g., C, was reported to stabilize the metastable $L1_0$-MnAl phase in the Mn-Al system[19], the Ag addition to Co-Pd seems to have no significant effect to obtain metastable $L1_0$-CoPd phase.

Figure 4 shows the RHEED patterns of $(CoPt)_{100-x}Ag_x$ with Ag amount of x = 0–15. The incidence of the electron beam was along [100] direction of MgO(001) substrate and the patterns were taken after the deposition of CoPt-Ag films. For x = 0, streak patterns with a space corresponding to the in-plane lattice spacing of CoPt were observed. The "vertical" streak pattern means slightly broadened reciprocal

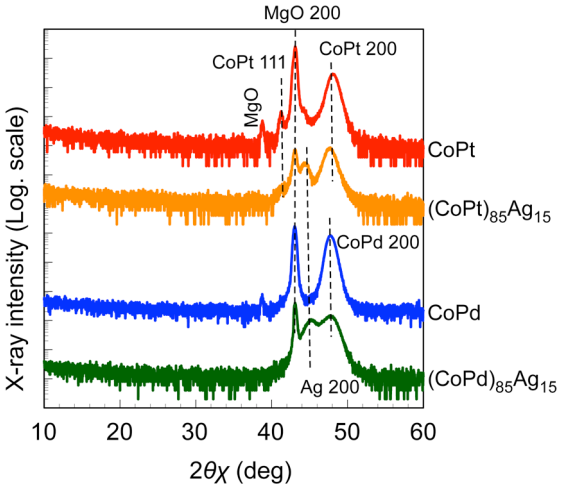

Fig. 3 In-plane ϕ–$2\theta\chi$ XRD profiles of $(CoPt)_{100-x}Ag_x$ and $(CoPd)_{100-x}Ag_x$ alloy films (x = 0 and 15) grown at 300°C. X-ray scattering vector is parallel to MgO [100] direction.

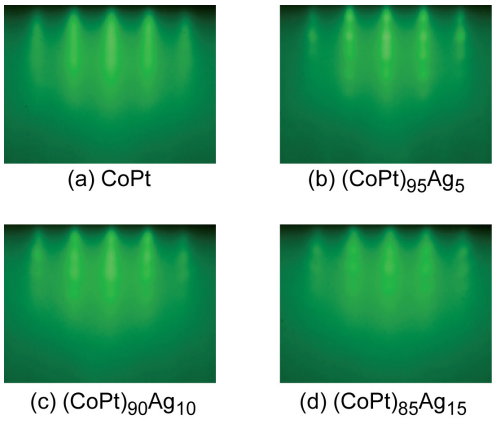

Fig. 4 RHEED patterns of $(CoPt)_{100-x}Ag_x$ grown at 300°C with Ag amounts of (a) x = 0, (b) 5, (c) 10, and (d) 15. The incidence of electron beam was along [100] direction of MgO(001) substrate. All patterns were taken after deposition of CoPt-Ag films.

lattice rods of CoPt, indicating rather flat surface of CoPt with atomic steps. With increasing the Ag content, the RHEED pattern changed from streaks to vertically aligned spots. This means the incident electrons passed inside the CoPt crystals, and thus indicates the granular growth of the CoPt-Ag. The AFM images of $(CoPt)_{95}Ag_5$ and $(CoPt)_{85}Ag_{15}$ are shown in Figs. 5 (a) and (b), respectively. With increasing the Ag content, the granular growth of the CoPt-Ag was confirmed, which coincides well with the RHEED observation. A similar granular growth by the addition of Ag was also confirmed in CoPd-Ag films. The granular structures of CoPt-Ag and CoPd-Ag are considered to be induced by the segregation of Ag from CoPt or CoPd, and we consider the Ag covers CoPt or CoPd grains, forming core/shell structure as observed in the FePt-Ag:C film[14]. White protrusions in Fig. 5 (b) are quite similar to Ag re-precipitates at the top of the FePt-oxide film reported by Yang *et al.*[20]. In such case, the actual Ag content in

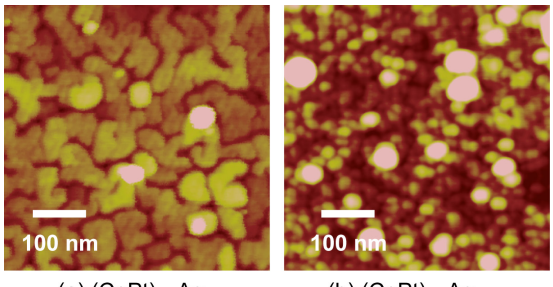

Fig. 5 AFM images of $(CoPt)_{95}Ag_5$ and $(CoPt)_{85}Ag_{15}$ grown at 300°C. Image area is 500 nm × 500 nm and vertical scale of image is 20 nm. Mean roughness R_a of image is (a) 1.47 nm and (b) 2.26 nm.

the CoPt-Ag may be smaller than the designed value. A similar granular growth by the addition of Ag was also confirmed in CoPd-Ag films.

3.2 Magnetic properties

The structural variations of CoPt-Ag and CoPd-Ag strongly affect their magnetic properties. Figure 6 shows hysteresis loops of $(CoPt)_{100-x}Ag_x$ and $(CoPd)_{100-x}Ag_x$, where the external field was applied parallel and perpendicular to the film plane. Figure 7 shows the Ag content dependence of the PMA, K_u, of CoPt-Ag and CoPd-Ag films, where the K_u was estimated from the torque curve applying a magnetic field of 15 kOe. For comparison, the K_u of the previously reported FePt-Ag and FePd-Ag are also shown in the same figure. For the CoPt-Ag, the increases of PMA and coercivity were found by the addition of Ag with an amount of 5 at. % as shown in Fig. 6 (b) and Fig. 7. However, for the CoPd-Ag, Ag addition reduced the PMA (see Fig. 7) and did not contribute to enhance the coercivity as shown in Fig. 6 (d)–(f). Interestingly, the CoPd film has some PMA and coercivity, which may be related to the long range order structure along CoPd [001] direction as discussed in Fig. 2. The variations of the magnetic properties of CoPt and CoPd with Ag content will be explained by the structural variation. For CoPt-Ag, Ag addition promotes $L1_0$ ordering, and Ag

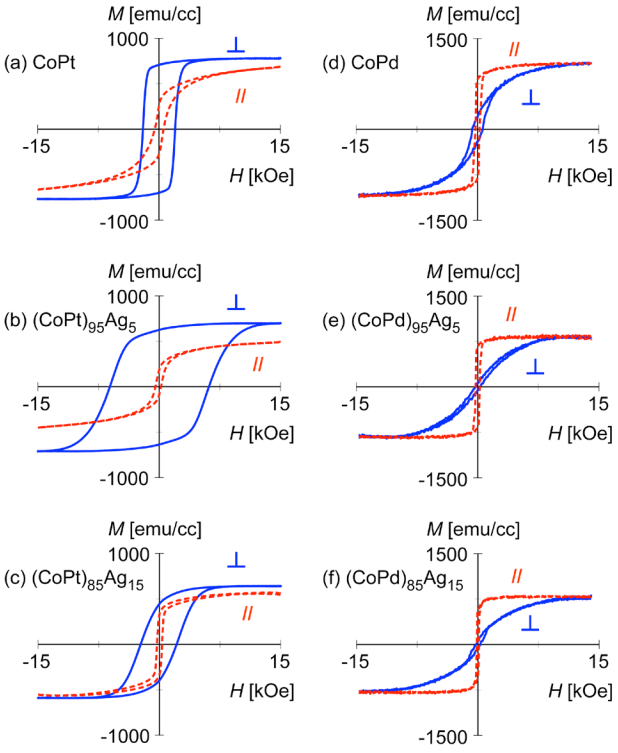

Fig. 6 Hysteresis loops of (a)–(c) $(CoPt)_{100-x}Ag_x$ and (d)–(f) $(CoPd)_{100-x}Ag_x$, where the external field was applied parallel and perpendicular to the film plane. Ag contents are (a), (d) x = 0, (b), (e) x = 5, and (c), (f) x =15.

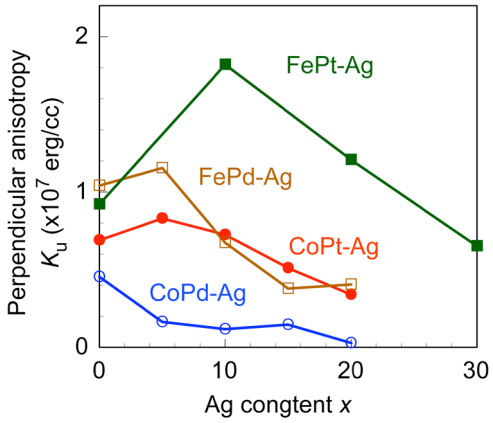

Fig. 7 Ag content dependence of perpendicular anisotropy K_u of CoPt-Ag and CoPd-Ag films, where K_u was estimated from torque curve applying a magnetic field of 15 kOe. For comparison, the K_u of the previously reported FePt-Ag grown at 250°C and FePd-Ag grown at 400°C are also shown[12].

atoms are considered to segregate from CoPt, which will make the $L1_0$-CoPt grains smaller as observed in Figs. 4 and 5. These structural variations will increase the PMA and coercivity of the CoPt-Ag films. On the other hand, Ag did not assist the formation of the $L1_0$ phase CoPd, which does not contribute to enhance the PMA and coercivity even though the granular growth was promoted by the Ag addition.

By comparing these results with those of the previously reported FePt-Ag and FePd-Ag[12], we found a similarity between FePt-Ag and CoPt-Ag. For both alloys, Ag addition enhanced their PMA and coercivity as shown in Fig. 7 and Ref. 12), owing that the Ag addition promoted the $L1_0$ ordering and granular growth. Also, there exists a similarity between FePd-Ag and CoPd-Ag; Ag addition did not contribute to enhance the coercivity in both alloys. However, there is a difference between FePd-Ag and CoPd-Ag. For FePd-Ag, the Ag tend to form an alloy with FePd, which lowers the coercivity even though its PMA slightly increases with the Ag addition of 5 at. % due to the increase of $L1_0$ ordering. For CoPd-Ag, the Ag atoms segregate from the CoPd, which makes the grains smaller, but the Ag does not contribute to promote $L1_0$ ordering.

4. Conclusion

The effect of Ag addition to CoPt and CoPd on their crystal structures and magnetic properties was investigated, and the results were compared with those of previously reported FePt-Ag and FePd-Ag for the systematic understanding of the effect of the Ag addition. It was confirmed that Ag atoms in the CoPt segregate from CoPt, which promotes $L1_0$ ordering and granular growth of CoPt. Such structural variations improved the magnetic properties of CoPt for a

perpendicular recording medium, e.g., increases of PMA and coercivity. These tendencies were similar to the results of FePt-Ag, in which Ag segregation effectively increases PMA and coercivity of FePt. On the other hand, Ag addition does not contribute to the increase of coercivity of CoPd, which is similar to the result of FePd-Ag. However, the microstructure of CoPd-Ag is different from that of FePd-Ag. For CoPd-Ag, Ag atoms segregate from CoPd, but do not assist the formation of the $L1_0$ CoPd phase. On the other hand, for FePd-Ag, Ag tends to form an alloy with FePd, which slightly promote the $L1_0$ ordering of FePd but does not contribute to the granular growth. From these results, it is considered that the reason why Ag is an effective material to obtain high ordered $L1_0$ phase and small sized grains is a low solubility of Ag to FePt and CoPt as well as a low surface energy of Ag, which will be effective to make core/shell structure as reported in Ref. 14).

Acknowledgements The authors would like to thank Mr. M. Kumazawa of Nagoya University for his assistance in the experiments. The authors are grateful for the financial support by Grant-in-Aids for Scientific Research from the Ministry of Education, Culture, Sports, Science and Technology.

References

1) P. Lu and S. H. Charap: *IEEE Trans. Magn.*, **31**, 2767 (1995).
2) D. Weller, A. Moser, L. Folks, M. E. Best, W. Lee, M. F. Toney, M. Schwickert, J. U. Thiele, and M. F. Doerner: *IEEE Trans. Magn.*, **36**, 10 (2000).
3) T. Maeda, T. Kai, A. Kikitsu, T. Nagase, and J. Akiyama: *Appl. Phys. Lett.*, **80**, 2147 (2002).
4) C. L. Platt, K. W. Wierman, E. B. Svedberg, R. Veerdonk, J. K. Howard, A. G. Roy, and D. E. Laughlin: *J. Appl. Phys.*, **92**, 6104 (2002).
5) K. Kang, T. Yang, and T. Suzuki: *IEEE Trans. Magn.*, **38**, 2039 (2002).
6) Y. Shao, M. L. Yan, and D. J. Sellmyer: *J. Appl. Phys.*, **93**, 8152 (2003).
7) C. Chen, O. Kitakami, S. Okamoto, and Y. Shimada: *Appl. Phys. Lett.*, **76**, 3218 (2000).
8) V. Karanasos, I. Panagiotopoulos, D. Niarchos, H. Okumura, and G. C. Hadjipanayis: *Appl. Phys. Lett.*, **79**, 1255 (2001).
9) B. Li, W. Liu, X. G. Zhao, S. Ma, W. J. Gong, J. N. Feng, F. Wang, and Z. D. Zhang: *Mater. Lett.*, **100**, 58 (2013).
10) T. Konagai, Y. Kitahara, T. Itoh, T. Kato, S. Iwata, and S. Tsunashima: *J. Magn. Magn. Mater.*, **310**, 2662 (2007).
11) R. Ikeda, M. Kagami, T. Kato, S. Iwata, and S. Tsunashima: *J. Magn. Soc. Jpn.*, **33**, 493 (2009).
12) Y. Tokuoka, Y. Seto, T. Kato, and S. Iwata: *J. Appl. Phys.*, **115**, 17B716 (2014).
13) L. Zhang, Y. K. Takahashi, K. Hono, B. C. Stipe, J. -Y. Juang, and M. Grobis: *J. Appl. Phys.*, **109**, 07B703 (2011).
14) B. S. D. Ch. S. Varaprasad, Y. K. Takahashi, J. Wang, T. Ina, T. Nakamura, W. Ueno, K. Nitta, T. Uruga, and K. Hono: *Appl. Phys. Lett.*, **104**, 222403 (2014).
15) K. Ishida and T. Nishizawa, *Binary Alloy Phase Diagrams*, 2nd ed., vol. 2, (ASM International, 1990), pp. 1220–1223.
16) Y. Matsuo: *J. Phys. Soc. Jpn.*, **32**, 972 (1972).
17) S. Ogawa and D. Watanabe: *J. Phys. Soc. Jpn.*, **9**, 475 (1954).
18) D. Watanabe, S. Ogawa: *J. Phys. Soc. Jpn.*, **11**, 226 (1956).
19) W. H. Dreizler and A. Menth: *IEEE Trans. Magn.*, **MAG-16**, 534 (1980).
20) E. Yang, D. E. Laughlin, J. G. Zhu: *IEEE Trans. Magn.*, **46**, 2446 (2010).

Received Jul. 27, 2015; Accepted Oct. 28, 2015